# Convex Optimization for Spring Design of Parallel Elastic Actuators

Sicong Guo, Robert D. Gregg, and Edgar Bolívar-Nieto

***Abstract*— Elastic actuation can improve human-robot interaction and energy efficiency for wearable robots. Previous work showed that the energy consumption of series elastic actuators can be a convex function of the series spring compliance. This function is useful to optimally select the series spring compliance that reduces the motor energy consumption. However, series springs have limited influence on the motor torque, which is a major source of the energy losses due to the associated Joule heating. Springs in parallel to the motor can significantly modify the motor torque and therefore reduce Joule heating, but it is unknown how to design springs that globally minimize energy consumption for a given motion of the load. In this work, we introduce the stiffness design of linear and nonlinear parallel elastic actuators via convex optimization. We show that the energy consumption of parallel elastic actuators is a convex function of the spring stiffness and compare the energy savings with that of optimal series elastic actuators. We analyze robustness of the solution in simulation by adding uncertainty of 20% of the RMS load kinematics and kinetics for the ankle, knee, and hip movements for level-ground human walking. When the winding Joule heating losses are dominant with respect to the viscous losses, our optimal PEA designs outperform SEA designs by further reducing the motor energy consumption up to 63%. Comparing to the linear PEA designs, our nonlinear PEA designs further reduced the motor energy consumption up to 31%. From our convex formulation, our global optimal nonlinear parallel elastic actuator designs give two different elongation-torque curves for positive and negative elongation, suggesting a clutching mechanism for the final implementation. In addition, the different torque-elongation profiles for positive and negative elongation for nonlinear parallel elastic actuators can cause sensitivity of the energy consumption to changes in the nominal load trajectory.**

## I. Introduction

Elastic actuation can enable a safe physical interaction between human and robots [1]–[4], and reduce the robot energy consumption [5], [6]. Series elastic actuators (SEAs) [7] and parallel elastic actuators (PEAs) [8], [9] are typical configurations for elastic actuation in applications requiring high torque-to-weight ratio and energy efficiency, such as robotic prostheses and exoskeletons. Through series connections with the motor, SEAs can modify the motor torque and velocity to reduce the motor peak power and improve the motor energy efficiency by proper tuning of the spring elongation [10], and also improve torque tracking at low frequencies [11]. For tasks compensating static torques at a joint, *e.g.*, gravity compensation, SEAs have limited abilities to reduce the motor energy consumption under large deviations of the initial position, due to their inability to provide the required static torque [8].

Our previous work formulated the SEA motor energy consumption as a convex function of the series spring compliance when the motion of the load is periodic [12], and proposed an optimization framework for robust-feasible SEA designs that satisfy all the actuator constraints despite uncertainties in load kinematics and kinetics, unmodeled dynamics, and limited manufacturing precision of the spring [13]. However, series elasticity does not reduce considerably the motor torque and the associated Joule heating losses [13].

PEAs also have the potential to reduce energy consumption and improve energy efficiency of the motor [14]. By placing the auxiliary spring in parallel with the motor, PEAs can compensate for gravitational loads and decrease the torque load on the motor [15], [16]. Such PEA designs can reduce the energy consumption by up-to 80% for prostheses [17], [18] and exoskeletons [19]. In addition, nonlinear PEAs can substantially lessen the actuator requirements for applications like prostheses [9].

### *Our contribution*

In this paper, we formulate the energy consumption of both linear and nonlinear PEAs as a convex function of the parallel spring stiffness (Sec. II). We use the convex formulation to find global optimal PEA designs, and compare the energy consumption of optimal PEAs against optimal SEAs in the presence of load kinematic and kinetic uncertainties (Sec. III). The paper has the following organization. Sec. II-A.1 will cover the electro-mechanical model of PEAs. Sec. II-A.2 will cover the actuator constraints of PEAs. Sec. II-B will cover the the convex formulation of energy consumption. Sec. III presents the energy consumption comparison between the rigid actuator, the optimal SEA, and the optimal PEA designs in the presence of tracking uncertainty in load kinematics and kinetics.

### *Notation*

In this paper, $\mathbb{R}_+$ and $\mathbb{R}_{++}$ denote the set of non-negative and positive real numbers. Bold lower-case characters represent column vectors in $\mathbb{R}^n$, and matrices in $\mathbb{R}^{n\times m}$ are in bold upper-case characters. The subindex in $\boldsymbol{a}_i$ refers to the $i$-th element of the vector $\boldsymbol{a}$. We use $\mathbf{1}$ to represent a vector with all its elements equal to 1 and dimensions to be interpreted by the context. We use $\boldsymbol{b} = \text{abs}(\boldsymbol{a})$ to represent a vector $\boldsymbol{b}$ with entries equal to the element-wise absolute value of $\boldsymbol{a}$. The term $\text{diag}(\boldsymbol{x})$ refers to the square matrix with the vector

This work was supported by the National Science Foundation under Award Numbers 1830360/1953908. S. Guo is with the Mechanical Engineering Department at the University of Michigan, Ann Arbor, MI 48109, USA; R. D. Gregg is with the Electrical Engineering and Computer Science Department and the Robotics Institute at the University of Michigan, Ann Arbor, MI 48109, USA; E. Bolívar-Nieto is with the Aerospace and Mechanical Engineering Department at the University of Notre Dame, Notre Dame, IN 46556, USA. Email: stevengu@umich.edu, {rgregg, ebolivar}@ieee.org

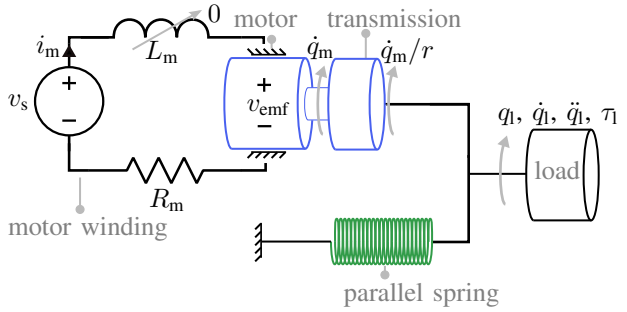


Fig. 1: Electro-mechanical diagram of an PEA. PEA refers to the combination of electric motor, mechanical transmission, and the spring in parallel connection with the load. (1) and (3) model the PEA's dynamics.

$\boldsymbol{x}$ along the diagonal. The matrix inequality $\boldsymbol{A} \succcurlyeq 0$ indicates that the matrix $\boldsymbol{A}$ is positive semidefinite.

## II. Optimal stiffness design of PEAs

In this section, we derive the electro-mechanical model of PEAs in Sec. II-A.1, and formulate the motor energy consumption of PEAs for both linear and nonlinear spring designs using the electro-mechanical model (Fig. 1). We formulate the motor energy consumption assuming that: i) the load kinematics and kinetics are periodic; ii) the inertial and viscous friction torques fully capture the dynamics of the transmission, *e.g.*, backlash and Coulomb friction are negligible; and iii) the winding temperature does not change significantly during operation.

### A. Dynamic model and actuator constraints of PEAs

*1) Electro-mechanical modeling:* Similar to the derivation of the electro-mechanical model in [8], [13] and using the Newton–Euler equations, we derive the equations of motion of the motor as:

$$\tau_m = I_m \ddot{q}_m + b_m \dot{q}_m - \frac{1}{r}(\tau_l + \tau_p), \tag{1}$$

$$\tau_p = -k_p \delta_p = -k_p q_l, \tag{2}$$

where $I_m \in \mathbb{R}_{++}$ is the rotor inertia of the motor; $b_m \in \mathbb{R}_{++}$ the motor's viscous friction coefficient; $r \in \mathbb{R}_{++}$ the reduction ratio of the transmission; $q_m, \dot{q}_m, \ddot{q}_m \in \mathbb{R}$ are the position, velocity, and acceleration of the motor, respectively; $\tau_p, \tau_m, \tau_l \in \mathbb{R}$ are the parallel spring torque, motor's electromagnetic torque, and load torque, respectively; $k_p \in \mathbb{R}_{++}$ is the stiffness of the parallel spring. The load trajectory is assumed to be known with some uncertainty and is defined as the set of variables $q_l, \dot{q}_l, \ddot{q}_l, \tau_l$.

Using the Kirchhoff's voltage law across the motor's winding, we model the electrical behavior of the PEA's motor with the following equation:

$$\begin{aligned} v_s &= i_m R_m + L_m \frac{di_m}{dt} + v_{emf}, \\ &\simeq i_m R_m + v_{emf} \end{aligned} \tag{3}$$

where $v_s \in \mathbb{R}$ is the voltage of the source, $i_m \in \mathbb{R}$ is the motor current, $R_m \in \mathbb{R}_{++}$ is the motor resistance, $L_m \in \mathbb{R}_{++}$ is the motor inductance, and $v_{emf} \in \mathbb{R}$ is the electromotive voltage of the motor. Similar to [20], we assume that the voltage drop across the motor's inductance is negligible compared to the voltage drop across the winding resistance. In SI units, the electromagnetic torque and electromotive voltage relate to motor current and speed as follows:

$$\tau_m = k_t i_m, \;\; v_{emf} = k_t \dot{q}_m, \tag{4}$$

where $k_t \in \mathbb{R}_{++}$ is the motor torque constant. Substituting the electromotive voltage and motor current in (4) into (3), we express electromagnetic torque as a function of supplied voltage and motor speed

$$\tau_m = v_s \frac{k_t}{R_m} - \dot{q}_m \frac{k_t^2}{R_m}. \tag{5}$$

In this paper, we will use the motor constant $k_m = k_t R_m^{-1/2}$ to calculate Joule heat losses in Sec. II-B. This electro-mechanical model (3) and (5) also applies to brushless permanent magnet DC motors, by using the direct-quadrature transformation [21], [22].

*2) Actuator constraints as functions of spring stiffness:* Similar to the case of SEA covered in [13], the PEA's motor and spring also have four types of actuator constraints: i) the RMS motor torque should not exceed the *continuous torque*, *i.e.*, $\text{rms}(\boldsymbol{\tau}_m) \leq \tau_{cont}$ to constrain the motor winding temperature; ii) the motor velocity should not exceed the maximum velocity, *i.e.*, $|\dot{q}_m| \leq \dot{q}_{max}$ to constrain the motor velocity; iii) the motor torque should not exceed the maximum motor torque, *i.e.*, $|\tau_m| \leq \tau_{max}$; and iv) the motor torque and velocity should satisfy the inequality [23]: $|\tau_m| \leq \frac{k_t}{R_m} v_s - \frac{k_t^2}{R_m} |\dot{q}_m|$.

### B. Convex formulation of energy consumption

In this section, we formulate the motor energy consumption for PEAs as a convex function of the parallel spring stiffness using the electro-mechanical model in Sec. II-A.1. Sec. II-B.1 and Sec. II-B.2 show convexity for linear and nonlinear parallel springs, respectively.

*1) Linear PEAs:* Neglecting backlash at the transmission, the motor position, velocity, and acceleration are

$$q_m = r q_l, \;\; \dot{q}_m = r \dot{q}_l, \;\; \ddot{q}_m = r \ddot{q}_l. \tag{6}$$

Substituting (6) and (2) into (1), we write the electromagnetic torque of the motor as the following affine function of spring stiffness:

$$\begin{aligned} \tau_m =& I_m \ddot{q}_m + b_m \dot{q}_m - \frac{1}{r}(\tau_l + \tau_p), \\ =& \underbrace{(q_l r^{-1})}_{a_{\tau_m}} k_p + \underbrace{(I_m r \ddot{q}_l + b_m r \dot{q}_l - \tau_l r^{-1})}_{b_{\tau_m}}. \end{aligned} \tag{7}$$

Joule heating and the rotor mechanical power represent most of the energy consumption of an electric motor [20]. Therefore, using (5), we derive the expression of motor

energy consumption as

$$\begin{aligned} E_{\mathrm{m}} &= \int_{t_0}^{t_f} i_{\mathrm{m}} v_{\mathrm{s}} dt, \\ &= \int_{t_0}^{t_f} \Big( \underbrace{\frac{\tau_{\mathrm{m}}^2}{k_{\mathrm{m}}^2}}_{\substack{\text{Winding} \\ \text{Joule} \\ \text{heating}}} + \underbrace{\tau_{\mathrm{m}} \dot{q}_{\mathrm{m}}}_{\substack{\text{Rotor} \\ \text{mechanical} \\ \text{power}}} \Big) dt, \\ &= \int_{t_0}^{t_f} \left[ \frac{\tau_{\mathrm{m}}^2}{k_{\mathrm{m}}^2} + \left( I_{\mathrm{m}} \ddot{q}_{\mathrm{m}} + b_{\mathrm{m}} \dot{q}_{\mathrm{m}} - \frac{1}{r}(\tau_{\mathrm{l}} + \tau_{\mathrm{p}}) \right) \dot{q}_{\mathrm{m}} \right] dt, \\ &= \int_{t_0}^{t_f} \left( \frac{\tau_{\mathrm{m}}^2}{k_{\mathrm{m}}^2} + b_{\mathrm{m}} \dot{q}_{\mathrm{m}}^2 - \tau_{\mathrm{l}} \dot{q}_{\mathrm{l}} \right) dt. \end{aligned} \tag{8}$$

where we assume that the load kinematics and kinetics are periodic and the parallel spring is conservative. Thus, for periodic motion, the energy from the inertial torques becomes zero and there is no energy stored or dissipated by the spring.

Substituting (6) and (7) into (8), we write the motor energy consumption as the following quadratic function of the parallel spring stiffness:

$$\begin{aligned} E_{\mathrm{m}} &= \int_{t_0}^{t_f} \left( \frac{\tau_{\mathrm{m}}^2}{k_{\mathrm{m}}^2} + b_{\mathrm{m}} \dot{q}_{\mathrm{m}}^2 - \tau_{\mathrm{l}} \dot{q}_{\mathrm{l}} \right) dt, \\ &= a_0 k_{\mathrm{p}}^2 + 2 b_0 k_{\mathrm{p}} + c_0 \end{aligned} \tag{9}$$

where

$$\begin{aligned} a_0 &= \int_{t_0}^{t_f} \frac{a_{\tau_{\mathrm{m}}}^2}{k_{\mathrm{m}}^2} dt, \\ b_0 &= \int_{t_0}^{t_f} \frac{a_{\tau_{\mathrm{m}}} b_{\tau_{\mathrm{m}}}}{k_{\mathrm{m}}^2} dt, \\ c_0 &= \int_{t_0}^{t_f} \left( \frac{b_{\tau_{\mathrm{m}}}^2}{k_{\mathrm{m}}^2} + b_{\mathrm{m}} r^2 \dot{q}_{\mathrm{l}}^2 - \tau_{\mathrm{l}} \dot{q}_{\mathrm{l}} \right) dt. \end{aligned}$$

The second derivative of the quadratic function (9) is non-negative, *i.e.*, $d^2 E_{\mathrm{m}} / d k_{\mathrm{p}}^2 = 2 a_0 \geq 0$; thus, (9) is a convex function of $k_{\mathrm{p}}$ [24].

We formulate the actuator constraints covered in Sec. II-A.2 as affine and quadratic inequalities of the parallel spring stiffness $k_{\mathrm{p}}$. The motor kinematics are independent of $k_{\mathrm{p}}$, as shown in (6). Therefore, we only consider actuator constraints on: i) the RMS motor torque; ii) the motor torque; and iii) the motor torque and velocity. In our formulation, we rewrite (6) and (7) in vector form, discretizing time in $n$ samples,

$$\boldsymbol{q}_{\mathrm{m}} = r \boldsymbol{q}_{\mathrm{l}}, \;\; \dot{\boldsymbol{q}}_{\mathrm{m}} = r \dot{\boldsymbol{q}}_{\mathrm{l}}, \;\; \ddot{\boldsymbol{q}}_{\mathrm{m}} = r \ddot{\boldsymbol{q}}_{\mathrm{l}}, \tag{10}$$

$$\boldsymbol{\tau}_{\mathrm{m}} = \underbrace{(\boldsymbol{q}_{\mathrm{l}} r^{-1})}_{\boldsymbol{a}_{\tau_{\mathrm{m}}}} k_{\mathrm{p}} + \underbrace{(I_{\mathrm{m}} r \ddot{\boldsymbol{q}}_{\mathrm{l}} + b_{\mathrm{m}} r \dot{\boldsymbol{q}}_{\mathrm{l}} - \boldsymbol{\tau}_{\mathrm{l}} r^{-1})}_{\boldsymbol{b}_{\tau_{\mathrm{m}}}}. \tag{11}$$

We use (11) to write the RMS motor torque constraint as the following quadratic inequality of spring stiffness:

$$\begin{aligned} \sqrt{\boldsymbol{\tau}_{\mathrm{m}}^T \boldsymbol{\tau}_{\mathrm{m}} n^{-1}} &\leq \tau_{\mathrm{cont}}, \\ \boldsymbol{a}_{\tau_{\mathrm{m}}}^T \boldsymbol{a}_{\tau_{\mathrm{m}}} k_{\mathrm{p}}^2 + 2 \boldsymbol{b}_{\tau_{\mathrm{m}}}^T \boldsymbol{a}_{\tau_{\mathrm{m}}} k_{\mathrm{p}} + \boldsymbol{b}_{\tau_{\mathrm{m}}}^T \boldsymbol{b}_{\tau_{\mathrm{m}}} &\leq \tau_{\mathrm{cont}}^2 n. \end{aligned} \tag{12}$$

Similarly, we use (11) and (10) to write the motor torque, and torque-velocity constraints as the following affine inequality of spring stiffness:

$$\begin{bmatrix} \boldsymbol{a}_{\tau_{\mathrm{m}}} \\ -\boldsymbol{a}_{\tau_{\mathrm{m}}} \end{bmatrix} k_{\mathrm{p}} \leq \begin{bmatrix} \mathbf{1} \tau_{\max} - \boldsymbol{b}_{\tau_{\mathrm{m}}} \\ \mathbf{1} \tau_{\max} + \boldsymbol{b}_{\tau_{\mathrm{m}}} \end{bmatrix}, \tag{13}$$

$$\begin{bmatrix} \boldsymbol{a}_{\tau_{\mathrm{m}}} \\ \boldsymbol{a}_{\tau_{\mathrm{m}}} \\ -\boldsymbol{a}_{\tau_{\mathrm{m}}} \\ -\boldsymbol{a}_{\tau_{\mathrm{m}}} \end{bmatrix} k_{\mathrm{p}} \leq \begin{bmatrix} \mathbf{1} k_{\mathrm{t}} R_{\mathrm{m}}^{-1} v_{\mathrm{s}} - \boldsymbol{b}_{\tau_{\mathrm{m}}} - r k_{\mathrm{t}}^2 R_{\mathrm{m}}^{-1} \dot{\boldsymbol{q}}_{\mathrm{l}} \\ \mathbf{1} k_{\mathrm{t}} R_{\mathrm{m}}^{-1} v_{\mathrm{s}} - \boldsymbol{b}_{\tau_{\mathrm{m}}} + r k_{\mathrm{t}}^2 R_{\mathrm{m}}^{-1} \dot{\boldsymbol{q}}_{\mathrm{l}} \\ \mathbf{1} k_{\mathrm{t}} R_{\mathrm{m}}^{-1} v_{\mathrm{s}} + \boldsymbol{b}_{\tau_{\mathrm{m}}} - r k_{\mathrm{t}}^2 R_{\mathrm{m}}^{-1} \dot{\boldsymbol{q}}_{\mathrm{l}} \\ \mathbf{1} k_{\mathrm{t}} R_{\mathrm{m}}^{-1} v_{\mathrm{s}} + \boldsymbol{b}_{\tau_{\mathrm{m}}} + r k_{\mathrm{t}}^2 R_{\mathrm{m}}^{-1} \dot{\boldsymbol{q}}_{\mathrm{l}} \end{bmatrix}. \tag{14}$$

To simplify notation, we lump the affine inequalities (13), and (14) as

$$\boldsymbol{M}_{\mathrm{l}} k_{\mathrm{p}} \leq \boldsymbol{p}_{\mathrm{l}}, \tag{15}$$

where $\boldsymbol{M}_{\mathrm{l}}, \boldsymbol{p}_{\mathrm{l}} \in \mathbb{R}^m$, and $m$ is the number of rows that results from stacking the affine inequalities vertically. The inequalities (15) and (12) represent our complete set of constraints.

The optimal linear parallel spring that minimizes energy consumption is the solution to the following convex optimization program:

$$\begin{aligned} \underset{k_{\mathrm{p}}}{\text{minimize}} \quad & a_0 k_{\mathrm{p}}^2 + 2 b_0 k_{\mathrm{p}} + c_0 \\ \text{subject to} \quad & \boldsymbol{a}_{\tau_{\mathrm{m}}}^T \boldsymbol{a}_{\tau_{\mathrm{m}}} k_{\mathrm{p}}^2 + 2 \boldsymbol{b}_{\tau_{\mathrm{m}}}^T \boldsymbol{a}_{\tau_{\mathrm{m}}} k_{\mathrm{p}} + \boldsymbol{b}_{\tau_{\mathrm{m}}}^T \boldsymbol{b}_{\tau_{\mathrm{m}}} \leq \tau_{\mathrm{cont}}^2 n, \\ & \boldsymbol{M}_{\mathrm{l}} k_{\mathrm{p}} \leq \boldsymbol{p}_{\mathrm{l}}. \end{aligned} \tag{16}$$

*2) Nonlinear PEAs:* In order to formulate the convexity of the motor energy consumption for nonlinear PEAs, we discretize the continuous-time spring stiffness using $n$ samples. The expression for the discrete-time spring stiffness vector, $\boldsymbol{k}_{\mathrm{p}} \in \mathbb{R}_+^n$, is:

$$\begin{aligned} \boldsymbol{k}_{\mathrm{p}i} &= -\frac{d \boldsymbol{\tau}_{\mathrm{p}i}}{d \boldsymbol{\delta}_{\mathrm{p}i}}, \\ &= -\frac{\dot{\boldsymbol{\tau}}_{\mathrm{p}i}}{\dot{\boldsymbol{\delta}}_{\mathrm{p}i}}, i = 1, \ldots, n. \end{aligned}$$

This definition applies for $\dot{\boldsymbol{\delta}}_{\mathrm{p}i} \neq 0$. For an energetically conservative spring, $\dot{\boldsymbol{\delta}}_{\mathrm{p}i} = 0$ implies that $\dot{\boldsymbol{\tau}}_{\mathrm{p}i} = 0$.

Utilizing the electro-mechanical model in Sec. II-A.1, we derive the motor velocity and acceleration as

$$\dot{\boldsymbol{q}}_{\mathrm{m}} = \boldsymbol{a}, \;\; \ddot{\boldsymbol{q}}_{\mathrm{m}} = \boldsymbol{c}, \tag{17}$$

where $\boldsymbol{a} = \dot{\boldsymbol{q}}_{\mathrm{l}} r$ and $\boldsymbol{c} = \ddot{\boldsymbol{q}}_{\mathrm{l}} r$. Substituting (17) into (1), we derive the motor's electromagnetic torque as

$$\boldsymbol{\tau}_{\mathrm{m}} = \boldsymbol{e} + \boldsymbol{F} \boldsymbol{k}_{\mathrm{p}}, \tag{18}$$

where $\boldsymbol{e} = I_{\mathrm{m}} \boldsymbol{c} + b_{\mathrm{m}} \boldsymbol{a} - \boldsymbol{\tau}_{\mathrm{l}} r^{-1}$ and $\boldsymbol{F} = \mathrm{diag}(\boldsymbol{q}_{\mathrm{l}}) r^{-1}$.

Similar to [13], using numerical integration and substituting (17) and (18) into (8), we approximate the energy consumption as

$$\begin{aligned} E_{\mathrm{m}} &\approx \left( \boldsymbol{\tau}_{\mathrm{m}}^T \boldsymbol{\tau}_{\mathrm{m}} k_{\mathrm{m}}^{-2} + b_{\mathrm{m}} \dot{\boldsymbol{q}}_{\mathrm{m}}^T \dot{\boldsymbol{q}}_{\mathrm{m}} - \boldsymbol{\tau}_{\mathrm{l}}^T \dot{\boldsymbol{q}}_{\mathrm{l}} \right) \Delta t \\ &= \boldsymbol{k}_{\mathrm{p}}^T \boldsymbol{G} \boldsymbol{k}_{\mathrm{p}} + \boldsymbol{h} \boldsymbol{k}_{\mathrm{p}} + w, \end{aligned} \tag{19}$$

where

$$\begin{aligned}\boldsymbol{G} &= \left(\boldsymbol{F}^T\boldsymbol{F}k_{\mathrm{m}}^{-2}\right)\Delta t,\\ \boldsymbol{h} &= \left(2\boldsymbol{e}^T\boldsymbol{F}k_{\mathrm{m}}^{-2}\right)\Delta t,\\ w &= \left(\boldsymbol{e}^T\boldsymbol{e}k_{\mathrm{m}}^{-2} + b_{\mathrm{m}}\boldsymbol{a}^T\boldsymbol{a} - \boldsymbol{\tau}_{\mathrm{l}}^T\dot{\boldsymbol{q}}_{\mathrm{l}}\right)\Delta t.\end{aligned}$$

The Hessian of the quadratic function (19) is a positive semi-definite function of $\boldsymbol{k}_{\mathrm{p}}$, *i.e.*, $d^2E_{\mathrm{m}}/d\boldsymbol{k}_{\mathrm{p}}^2 = 2\boldsymbol{G} \succcurlyeq 0$. Thus the quadratic function (19) is a convex function of $\boldsymbol{k}_{\mathrm{p}}$ [24].

Similar to Sec. II-B.1, we formulate the RMS motor torque, the motor torque, and the motor torque-velocity constraints covered in Sec. II-A.2 as affine and quadratic inequalities of the discrete-time spring stiffness vector $\boldsymbol{k}_{\mathrm{p}}$. In our formulation, we use (18) to write the RMS motor torque constraint as the following quadratic inequality of spring stiffness:

$$\begin{aligned}\sqrt{\boldsymbol{\tau}_{\mathrm{m}}^T\boldsymbol{\tau}_{\mathrm{m}}n^{-1}} &\leq \tau_{\mathrm{cont}},\\ \boldsymbol{k}_{\mathrm{p}}^T\boldsymbol{F}^T\boldsymbol{F}\boldsymbol{k}_{\mathrm{p}} + 2\boldsymbol{e}^T\boldsymbol{F}\boldsymbol{k}_{\mathrm{p}} + \boldsymbol{e}^T\boldsymbol{e} &\leq \tau_{\mathrm{cont}}^2 n.\end{aligned} \tag{20}$$

Similarly, we use (17) and (18) to write the motor torque, and torque-velocity constraints as the following affine inequality of spring stiffness:

$$\begin{bmatrix}\boldsymbol{F}\\ -\boldsymbol{F}\end{bmatrix}\boldsymbol{k}_{\mathrm{p}} \leq \begin{bmatrix}\mathbf{1}\tau_{\max} - \boldsymbol{e}\\ \mathbf{1}\tau_{\max} + \boldsymbol{e}\end{bmatrix}, \tag{21}$$

$$\begin{bmatrix}\boldsymbol{F}\\ \boldsymbol{F}\\ -\boldsymbol{F}\\ -\boldsymbol{F}\end{bmatrix}\boldsymbol{k}_{\mathrm{p}} \leq \begin{bmatrix}\mathbf{1}k_{\mathrm{t}}R_{\mathrm{m}}^{-1}v_{\mathrm{s}} - \boldsymbol{e} - rk_{\mathrm{t}}^2R_{\mathrm{m}}^{-1}\dot{\boldsymbol{q}}_{\mathrm{l}}\\ \mathbf{1}k_{\mathrm{t}}R_{\mathrm{m}}^{-1}v_{\mathrm{s}} - \boldsymbol{e} + rk_{\mathrm{t}}^2R_{\mathrm{m}}^{-1}\dot{\boldsymbol{q}}_{\mathrm{l}}\\ \mathbf{1}k_{\mathrm{t}}R_{\mathrm{m}}^{-1}v_{\mathrm{s}} + \boldsymbol{e} - rk_{\mathrm{t}}^2R_{\mathrm{m}}^{-1}\dot{\boldsymbol{q}}_{\mathrm{l}}\\ \mathbf{1}k_{\mathrm{t}}R_{\mathrm{m}}^{-1}v_{\mathrm{s}} + \boldsymbol{e} + rk_{\mathrm{t}}^2R_{\mathrm{m}}^{-1}\dot{\boldsymbol{q}}_{\mathrm{l}}\end{bmatrix}. \tag{22}$$

To simplify notation, we lump the affine inequalities (21), and (22) as

$$\boldsymbol{M}_{\mathrm{n}}\boldsymbol{k}_{\mathrm{p}} \leq \boldsymbol{p}_{\mathrm{n}}, \tag{23}$$

where $\boldsymbol{M}_{\mathrm{n}} \in \mathbb{R}^{m\times n}$, $\boldsymbol{p}_{\mathrm{n}} \in \mathbb{R}^m$, and $m$ is the number of rows that results from stacking the affine inequalities vertically. (23) and (20) represent our complete set of constraints.

The optimal nonlinear parallel spring that minimizes energy consumption is the solution to the following convex optimization program:

$$\begin{aligned}\underset{\boldsymbol{k}_{\mathrm{p}}}{\text{minimize}} \quad & \boldsymbol{k}_{\mathrm{p}}^T\boldsymbol{G}\boldsymbol{k}_{\mathrm{p}} + \boldsymbol{h}\boldsymbol{k}_{\mathrm{p}} + w\\ \text{subject to} \quad & \boldsymbol{k}_{\mathrm{p}}^T\boldsymbol{F}^T\boldsymbol{F}\boldsymbol{k}_{\mathrm{p}} + 2\boldsymbol{e}^T\boldsymbol{F}\boldsymbol{k}_{\mathrm{p}} + \boldsymbol{e}^T\boldsymbol{e} \quad \leq \tau_{\mathrm{cont}}^2 n\\ & \boldsymbol{M}_{\mathrm{n}}\boldsymbol{k}_{\mathrm{p}} \leq \boldsymbol{p}_{\mathrm{n}}.\end{aligned} \tag{24}$$

## III. Simulation results and discussion

In this section, we used the convex optimization program (16) and (24) to minimize the energy consumption of PEAs accomplishing various tasks. We defined the motion tasks from the load position and torque trajectories for the ankle, knee, and hip joints of humans walking on level ground, as reported in [25] and discretized over $n = 1000$ samples. Each trajectory also satisfied our RMS torque, motor speed-torque, and spring elongation constraints. Table I summarizes the actuator parameters for our simulations. In all simulations, CVX (Matlab Software for Disciplined Convex Programming) executed the solvers Mosek [26] with precision settings `cvx_precision default`. The source code for all simulations is available in the GitHub repository, `https://github.com/UM-LoCoLab/Convex_Optimization_for_PEAs.git`.

TABLE I: PEA simulation parameters. These values match the knee-ankle actuators experimentally validated in [21].

| Parameter | Value |
|---|---|
| Motor inertia, $I_{\mathrm{m}}$ ($\mathrm{kg}\cdot\mathrm{m}^2$) | $1.2\times10^{-4}$ |
| Viscous friction, $b_{\mathrm{m}}$ ($\mathrm{N}\cdot\mathrm{m}\cdot\mathrm{s/rad}$) | $0.16\times10^{-3}$ |
| Transmission ratio, $r$ | 50 |
| Motor torque constant, $k_{\mathrm{t}}$ ($\mathrm{N}\cdot\mathrm{m/A}$) | 0.14 |
| Terminal resistance, $R_{\mathrm{m}}$ ($\Omega$) | 0.279 |
| Motor constant, $k_{\mathrm{m}}$ ($\mathrm{N}\cdot\mathrm{m}/(\mathrm{W}^2)$) | 0.265 |
| Max. velocity, $\dot{q}_{\max}$ ($\mathrm{rad/s}$) | 342.9 |
| Max. motor torque, $\tau_{\max}$ ($\mathrm{N}\cdot\mathrm{m}$) | 4.02 |
| Cont. torque, $\tau_{\mathrm{cont}}$ ($\mathrm{N}\cdot\mathrm{m}$) | 1.1 |
| Voltage, $V_m$ (V) | 48 |

For each motion task, we compared the motor energy consumption of optimal PEA designs with both the optimal SEA designs and rigid actuators. We generated the global optimal SEA designs by applying the method presented in [13]. The method in [13] minimizes the SEA version of the cost functions (9) and (19) when the spring is in series with the load, and the optimization variable is the spring compliance instead of stiffness.

In addition, to validate the robustness of our global optimal PEA designs under uncertainties in the kinematics and kinetics of the load, for each motion task, we simulated both ideal and imperfect trajectory tracking cases. We simulated the imperfect tracking cases with Monte Carlo simulations, by adding an additive uncertainty of 20% of the RMS load kinematics and kinetics for position, velocity, acceleration, and torque of the load. This uncertainty was a sample of a uniformly distributed probability distribution. Consequently, the variation over a stride for a specific joint could reach $20\%$ of the corresponding RMS value, which is comparable to the coefficient of variation reported in [25]. For each imperfect tracking case, we ran 10000 trials for every Monte Carlo simulation, and reported the energy consumptions with both the mean and standard deviation. The mean value of our random experiments converged within $\pm2\%$ deviation with this number of Monte Carlo trials.

TABLE II: Optimal linear spring stiffness designs for the ankle, knee, and hip movements for level-ground human walking (in N-m/rad). For these motion tasks, we used the load position and torque trajectories reported in [25]. The dash for walking knee movements under fast cadence represents that the global optimal linear PEA design is infeasible.

| | ankle | | hip | | knee | |
|---|---|---|---|---|---|---|
| Walking speed | SEA | PEA | SEA | PEA | SEA | PEA |
| slow | 154.6 | 249.1 | 406.4 | 40.2 | 133.2 | 7.27 |
| normal | 164.6 | 213.5 | 483.8 | 55.8 | 137.6 | 15.35 |
| fast | 195.3 | 179.4 | 460.7 | 95.2 | 430.8 | - |

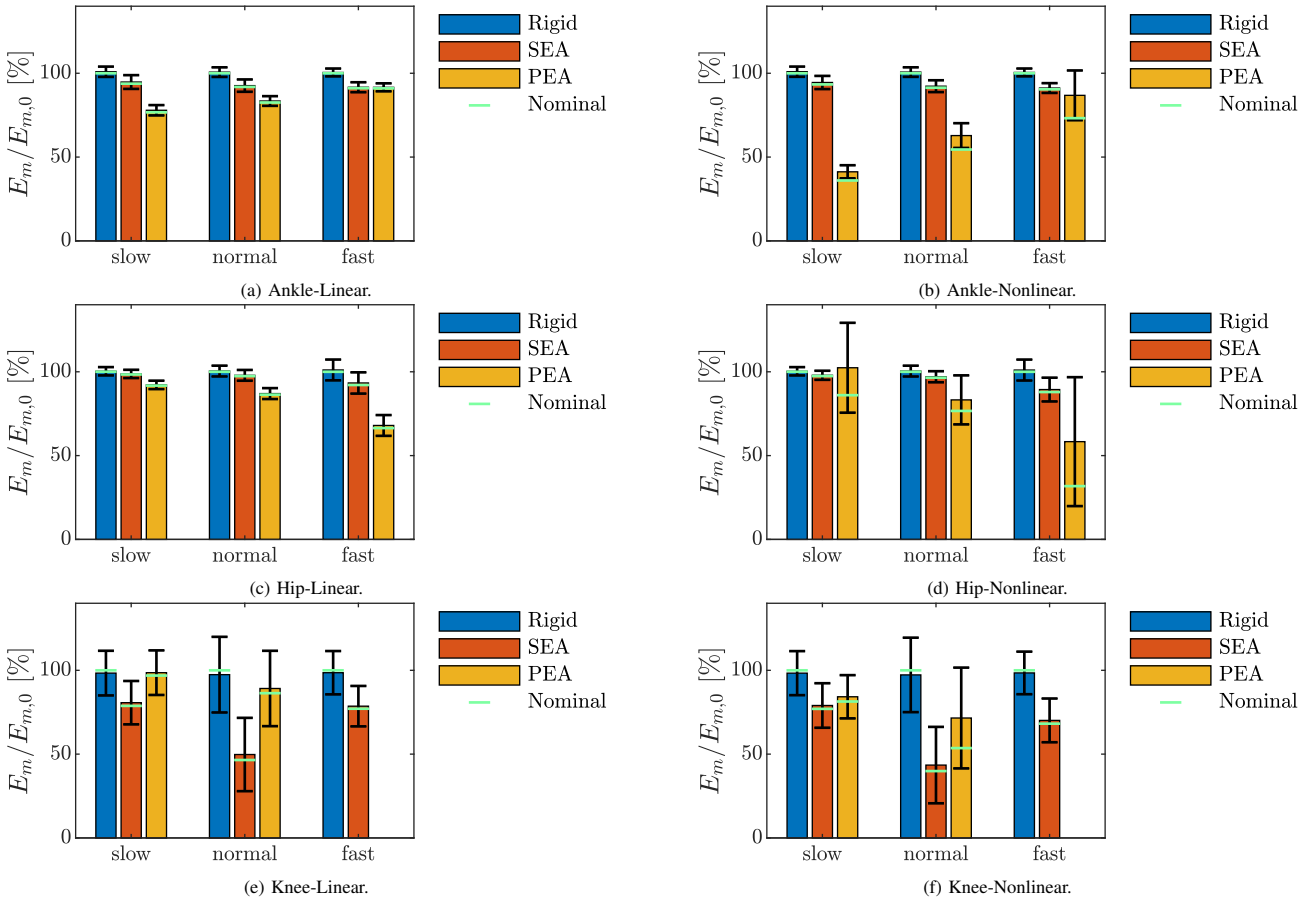


(a) Ankle-Linear. (b) Ankle-Nonlinear. (c) Hip-Linear. (d) Hip-Nonlinear. (e) Knee-Linear. (f) Knee-Nonlinear.

Fig. 2: Normalized energy consumption of the motor with linear (left) and nonlinear (right) spring designs compared to the energy consumption of the rigid actuator. We reported the values of linear spring stiffness in Table II. Each bar represents the mean value of energy consumption, and the green lines on each bar represent the nominal value of energy consumption with no tracking uncertainty. In addition, the error bars represent two times the standard deviation of energy consumption with tracking uncertainties. For the fast-walking knee motion, we found that both global optimal linear and nonlinear PEA designs were infeasible. Therefore, we left blank for the energy consumption of both linear and nonlinear PEAs.

### A. *Optimal PEAs for hip and ankle movements*

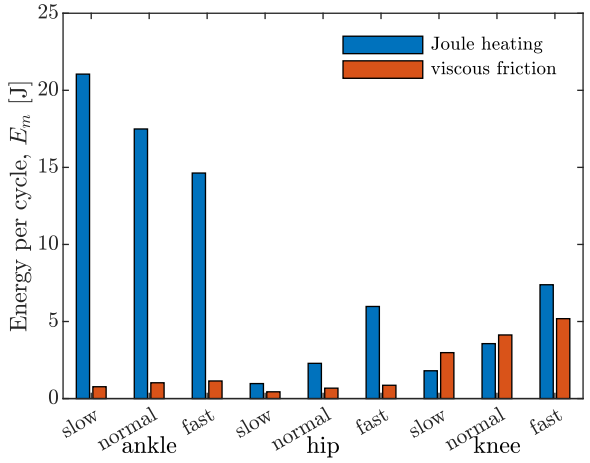


Fig. 3: The motor energy consumption from Joule heating and viscous friction. For ankle and hip movements, the ratio between the energy from Joule heating to viscous friction ranges from 2.2 to 27.4. For knee movements, the ratio between the energy from Joule heating to viscous friction for slow and normal cadences are 0.6 and 0.9, respectively.

*1) Linear PEAs:* The linear PEAs outperformed the nonlinear SEAs for hip and ankle movements by reducing the energy consumption of the motor up to $34\%$ from the rigid actuator case under ideal load kinematic and kinetic tracking, and up to $32\% \pm 6\%$ under the aforementioned uncertainties in the load kinematics and kinetics (Fig. 2a and Fig. 2c). The additional energy savings of PEAs were possible because the energy losses from Joule heating represented most of the energy losses during hip and ankle movements, as shown in Fig. 3. Parallel springs had a higher influence on the motor torque than series springs; thus, PEAs were advantageous to modify the associated Joule heating.

*2) Nonlinear PEAs:* The nonlinear PEAs outperformed the nonlinear SEAs for hip and ankle movements by reducing the energy consumption of the motor up to $64\%$ from the rigid actuator case under ideal load kinematics and kinetics tracking, and up to $59\% \pm 4\%$ in the presence of tracking uncertainty (Fig. 2b and Fig. 2d). Similar to the linear spring case in Sec. III-A.1, PEAs had more influence in motor torque and the corresponding Joule heating than the SEAs.

Our global optimal nonlinear PEA designs provided different elongation-torque curves for positive and negative elongations. For example, Fig. 4a shows an optimal PEA

design with a piece-wise expression of $\tau_p = f(\delta_p)$ for the hip movement under fast cadence, suggesting a clutched PEA design with a torque offset for the mechanical implementation. Fig. 4c illustrates the implications of this discontinuity in the motor torque by comparing the torque profiles for the linear and the nonlinear PEA.

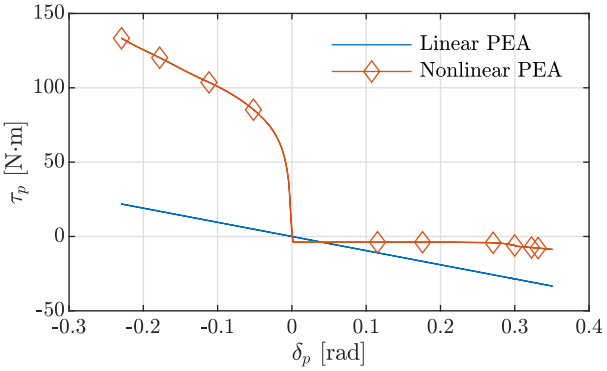


(a) Optimal linear and nonlinear parallel springs for the hip movement under fast cadence.

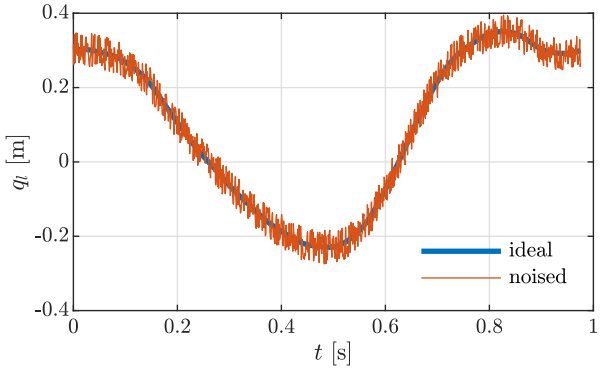


(b) Load position profile under both ideal and imperfect tracking cases.

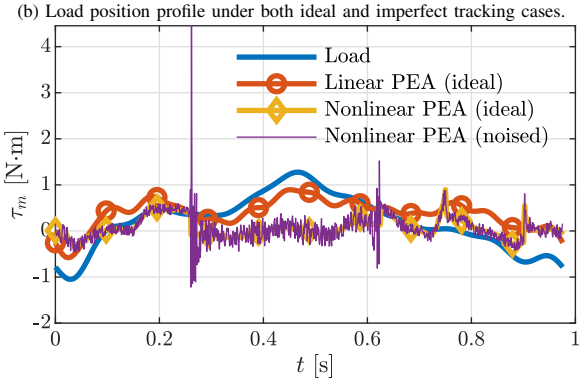


(c) Motor torque profile for the optimal linear and nonlinear PEA designs under ideal tracking, and the optimal nonlinear PEA design under imperfect tracking.

Fig. 4: Elongation-torque, load position, and motor torque profiles for the PEA designs optimized to perform the hip motion at fast cadence. Discontinuities in motor torque profile occurred at instances when the load position trajectory crossed zero. The uncertainties in load position when it crossed zero led to significant deviation in motor torque.

For hip motion, even though the nonlinear PEAs outperformed nonlinear SEAs under ideal tracking, the tracking uncertainty caused a large variation in the motor energy consumption, which could be higher than the nonlinear SEAs or even the rigid actuators. This sensitivity of the energy consumption to poor tracking was mostly due to the optimal torque-elongation PEA profile. Analyzing Fig. 4a, the stiffness of the PEA increased as $\delta_p \to 0^+$; however, the stiffness approached 0 as $\delta_p \to 0^-$. Such discontinuity can cause large variations in energy consumption, especially when the elongation of the spring is small in either direction, as a small deviation in $\delta_p$ would lead to a significant deviation in $\tau_p$. As shown in Fig. 4, when the load position trajectory crossed zero in Fig. 4b, *e.g.*, at 0.26 and 0.63 seconds, the added uncertainties caused large deviations from the nominal motor torque in Fig. 4c. In addition, large spring stiffness under negative elongation (Fig. 4a) led to large uncertainties in motor torque than under positive elongation. Ultimately, this piece-wise feature in the optimal torque-elongation PEA profile led to significant sensitivity of the motor energy consumption to poor tracking. In future work, we will add a constraint so that the torque-elongation curve of the spring is smooth.

### *B. Optimal PEAs for knee movements*

As shown in Fig. 2e, for the knee movements, the linear PEAs were able to reduce the energy consumption of the motor up to $14\%$ from the rigid actuator case under ideal load kinematics and kinetics tracking, and up to $11\% \pm 22\%$ under the aforementioned uncertainties in the load kinematics and kinetics. The nonlinear PEAs (Fig. 2f) were able to reduce the energy consumption of the motor up to $46\%$ from the rigid actuator case under ideal load kinematics and kinetics tracking, and up to $28\% \pm 30\%$ under the aforementioned uncertainties in the load kinematics and kinetics. The optimized PEA designs failed to outperform the optimal SEA designs in energy consumption reduction, since the energy losses from Joule heating were not dominant compared to that from viscous friction, as shown in Fig. 3. Since PEA designs cannot modify the motor velocity while SEA designs can, PEAs are not as advantageous as the SEAs for walking knee movements using the motor configuration in Table I. This fact also encourages the combination of serial and parallel springs, since such elastic actuator designs can modify both the motor torque and velocity simultaneously; thus, they are advantageous to further reduce the motor energy consumption for motion tasks with comparable energy losses from Joule heating and viscous friction.

### *C. Linear PEAs vs. Nonlinear PEAs*

For walking ankle movements under normal cadence, compared to the linear PEAs, the nonlinear PEAs further reduced the motor energy consumption around $34\%$ under ideal load kinematics and kinetics tracking, and around $25\% \pm 6\%$ in the presence of tracking uncertainty (Fig. 2a and Fig. 2b). For walking hip movements under normal cadence, compared to the linear PEAs, the nonlinear PEAs further reduced the motor energy consumption around $11\%$ under ideal load kinematics and kinetics tracking, and around $4\% \pm 13\%$ in the presence of tracking uncertainty (Fig. 2c and Fig. 2d). For walking knee movements under normal cadence, compared to the linear PEAs, the nonlinear PEAs further reduced the motor energy consumption up to $38\%$

under ideal load kinematics and kinetics tracking, and up to $20\% \pm 14\%$ in the presence of tracking uncertainty (Fig. 2e and Fig. 2f). Similar to the case in Sec. III-A.2, nonlinear PEAs had the potential to further reduce motor energy consumption from linear PEAs; however, the discontinuity in the torque-elongation PEA profile led to significant sensitivity of the energy consumption to poor tracking. Since trajectory tracking will always be prone to error for any motion task, it is beneficial to constraint the optimal nonlinear torque-elongation curve to be smooth.

## IV. Conclusions

We formulated the PEA motor energy consumption as a convex function of parallel spring stiffness, and compare the optimal PEA and SEA energy consumption in the presence of tracking uncertainties. In addition to ideal load kinematics and kinetics tracking cases, we also added an additive uncertainty of $20\%$ of the RMS load kinematics and kinetics for the ankle, knee, and hip movements for level-ground human walking. When the winding Joule heating losses are dominant with respect to the viscous losses, our optimal PEA designs outperform SEA designs by further reducing the motor energy consumption up to $63\%$. Comparing to the linear PEA designs, our nonlinear PEA designs further reduced the motor energy consumption up to $31\%$. From our convex formulation, the global optimal nonlinear parallel elastic actuator designs give two different elongation-torque curves for positive and negative elongation, suggesting a clutching mechanism for final implementation. In addition, the difference between the designs for positive and negative elongation for nonlinear parallel elastic actuators can cause large deviations from the ideal tracking case. These suggest further studies on robust optimal design of PEAs and experimental validations of such designs. They also suggest studies on a combination of series and parallel elastic actuators, and the corresponding convex formulation.

## References


[1] T. Lens and O. Von Stryk, "Investigation of safety in human-robot-interaction for a series elastic, tendon-driven robot arm," in *Proc. IEEE/RSJ International Conference on Intelligent Robots and Systems (IROS'12)*, Oct. 2012, pp. 411–422.

[2] J.-J. Park, Y.-J. Lee, J.-B. Song, and H.-S. Kim, "Safe joint mechanism based on nonlinear stiffness for safe human-robot collision," in *2008 IEEE International Conference on Robotics and Automation*, 2008, pp. 2177–2182.

[3] A. Bicchi and G. Tonietti, "Fast and "soft-arm" tactics [robot arm design]," *IEEE Robotics Automation Magazine*, vol. 11, no. 2, pp. 22–33, 2004.

[4] B. Vanderborght, A. Albu-Schaeffer, A. Bicchi, E. Burdet, D. Caldwell, R. Carloni, M. Catalano, O. Eiberger, W. Friedl, G. Ganesh, M. Garabini, M. Grebenstein, G. Grioli, S. Haddadin, H. Hoppner, A. Jafari, M. Laffranchi, D. Lefeber, F. Petit, S. Stramigioli, N. Tsagarakis, M. Van Damme, R. Van Ham, L. Visser, and S. Wolf, "Variable impedance actuators: A review," *Robotics and Autonomous Systems*, vol. 61, no. 12, pp. 1601–1614, 2013.

[5] B. Vanderborght, R. V. Ham, D. Lefeber, T. G. Sugar, and K. W. Hollander, "Comparison of mechanical design and energy consumption of adaptable, passive-compliant actuators," *The International Journal of Robotics Research*, vol. 28, no. 1, pp. 90–103, 2009.

[6] A. Velasco, G. M. Gasparri, M. Garabini, L. Malagia, P. Salaris, and A. Bicchi, "Soft-actuators in cyclic motion: Analytical optimization of stiffness and pre-load," in *2013 13th IEEE-RAS International Conference on Humanoid Robots (Humanoids)*, 2013, pp. 354–361.

[7] G. Pratt and M. Williamson, "Series elastic actuators," in *Proceedings 1995 IEEE/RSJ International Conference on Intelligent Robots and Systems. Human Robot Interaction and Cooperative Robots*, vol. 1, 1995, pp. 399–406 vol.1.

[8] P. Beckerle, T. Verstraten, G. Mathijssen, R. Furnémont, B. Vanderborght, and D. Lefeber, "Series and parallel elastic actuation: Influence of operating positions on design and control," *IEEE/ASME Transactions on Mechatronics*, vol. 22, no. 1, pp. 521–529, 2017.

[9] J. Realmuto, G. Klute, and S. Devasia, "Nonlinear Passive Cam-Based Springs for Powered Ankle Prostheses," *Journal of Medical Devices*, vol. 9, no. 1, 03 2015.

[10] D. Dong, W. Ge, B. Convens, Y. Sun, T. Verstraten, and B. Vanderborght, "Design, optimization and energetic evaluation of an efficient fully powered ankle-foot prosthesis with a series elastic actuator," *IEEE Access*, vol. 8, pp. 61 491–61 503, 2020.

[11] D. W. Robinson, "Design and Analysis of Series Elasticity in Closed-loop Actuator Force Control," Ph.D. dissertation, Massachusetts Institute of Technology, July 2000.

[12] E. A. Bolívar-Nieto, G. C. Thomas, E. Rouse, and R. D. Gregg, "Convex optimization for spring design in series elastic actuators: From theory to practice," in *Proc. IEEE International Conference on Intelligent Robots and Systems (IROS'21)*, Prague, Czech Republic, Sept. 2021, pp. x–x.

[13] E. A. Bolívar-Nieto, T. Summers, R. D. Gregg, and S. Rezazadeh, "A convex optimization framework for robust-feasible series elastic actuators," *Mechatronics*, vol. 79, p. 102635, 2021.

[14] M. Plooij and M. Wisse, "A novel spring mechanism to reduce energy consumption of robotic arms," in *2012 IEEE/RSJ International Conference on Intelligent Robots and Systems*, 2012, pp. 2901–2908.

[15] M. Grimmer, M. Eslamy, S. Gliech, and A. Seyfarth, "A comparison of parallel- and series elastic elements in an actuator for mimicking human ankle joint in walking and running," in *2012 IEEE International Conference on Robotics and Automation*, 2012, pp. 2463–2470.

[16] N. G. Tsagarakis, S. Morfey, H. Dallali, G. A. Medrano-Cerda, and D. G. Caldwell, "An asymmetric compliant antagonistic joint design for high performance mobility," in *2013 IEEE/RSJ International Conference on Intelligent Robots and Systems*, 2013, pp. 5512–5517.

[17] D. F. B. Haeufle, M. D. Taylor, S. Schmitt, and H. Geyer, "A clutched parallel elastic actuator concept: Towards energy efficient powered legs in prosthetics and robotics," in *2012 4th IEEE RAS EMBS International Conference on Biomedical Robotics and Biomechatronics (BioRob)*, 2012, pp. 1614–1619.

[18] T. Verstraten, L. Flynn, J. Geeroms, B. Vanderborght, and D. Lefeber, "On the electrical energy consumption of active ankle prostheses with series and parallel elastic elements," in *2018 7th IEEE International Conference on Biomedical Robotics and Biomechatronics (Biorob)*, 2018, pp. 720–725.

[19] Y. Zhu, J. Yang, H. Jin, X. Zang, and J. Zhao, "Design and evaluation of a parallel-series elastic actuator for lower limb exoskeletons," in *2014 IEEE International Conference on Robotics and Automation (ICRA)*, 2014, pp. 1335–1340.

[20] T. Verstraten, G. Mathijssen, R. Furnémont, B. Vanderborght, and D. Lefeber, "Modeling and design of geared dc motors for energy efficiency: Comparison between theory and experiments," *Mechatronics*, vol. 30, pp. 198–213, 2015.

[21] U. H. Lee, C.-W. Pan, and E. J. Rouse, "Empirical characterization of a high-performance exterior-rotor type brushless dc motor and drive," in *2019 IEEE/RSJ International Conference on Intelligent Robots and Systems (IROS)*, 2019, pp. 8018–8025.

[22] R. H. Park, "Two-reaction theory of synchronous machines generalized method of analysis-part i," *Transactions of the American Institute of Electrical Engineers*, vol. 48, no. 3, pp. 716–727, 1929.

[23] S. Rezazadeh and J. W. Hurst, "On the optimal selection of motors and transmissions for electromechanical and robotic systems," in *2014 IEEE/RSJ International Conference on Intelligent Robots and Systems*, 2014, pp. 4605–4611.

[24] S. Boyd and L. Vandenberghe, *Convex Optimization*. New York, NY: Cambridge University Press, New York, 2004.

[25] D. A. Winter, "Biomechanical motor patterns in normal walking," *Journal of Motor Behavior*, vol. 15, no. 4, pp. 302–330, 1983.

[26] M. ApS. (2021) Mosek optimization suite. [Online]. Available: https://docs.mosek.com/9.3/intro.pdf